European Journal of Mechanics B/Fluids 61 (2017) 25–32

Contents lists available at ScienceDirect

European Journal of Mechanics B/Fluids

journal homepage: www.elsevier.com/locate/ejmflu

Fluid flow and heat transfer of non-Newtonian nanofluid in a microtube considering slip velocity and temperature jump boundary conditions

Seyed Ali Sajadifar [a], Arash Karimipour [a,*], Davood Toghraie [b]

[a] Department of Mechanical Engineering, Najafabad Branch, Islamic Azad University, Najafabad, Iran

[b] Department of Mechanical Engineering, Khomeinishahr Branch, Islamic Azad University, Khomeinishahr, Iran

ARTICLE INFO

Article history:
Received 21 November 2015
Received in revised form
9 September 2016
Accepted 9 September 2016
Available online 8 October 2016

Keywords:
Microtube
Slip flow regime
Slip coefficient
Non-Newtonian nanofluid

ABSTRACT

Forced convection of non-Newtonian nanofluid, aqueous solution of carboxymethyl cellulose (CMC)–Aluminum oxide through a microtube is studied numerically. The length and diameter of tube are $L = 5$ mm and $D = 0.2$ mm, respectively which means the length is long enough compared to the diameter. The effects of different values of nanoparticles volume fraction, slip coefficient and Reynolds number are investigated on the slip velocity and temperature jump boundary conditions. Moreover the suitable validations are presented to confirm the achieved results accuracy. The results are shown as the dimensionless velocity and temperature profiles; however the profiles of local and averaged Nusselt number are also provided. It is seen that more volume fraction and slip coefficient correspond to higher Nusselt number especially at larger amounts of Re.

1. Introduction

Heat transfer plays a significant role in various applications. Technological advances have made high-efficiency heat transfer methods a requirement for research projects and industries. For example, cooling and heating, thermal sources and manufacturing processes such as foodstuff pasteurization, automobile manufacturing, pharmacy, transportation and development of microelectromechanical and nanoelectromechanical systems. In recent years, producing tools and devices in smaller dimensions has been targeted to improve their efficiency [1–4].

Improving efficiency is achieved through alteration of physical properties of agent fluids, changes in boundary conditions and the geometry of the flow. With technological advances and subsequent smaller electronic devices, research in fluid flow and heat transfer on microscale has attracted various practitioners. Recent breakthroughs in production of nanoparticles could be considered a change in improving heat transfer methods as smaller particles and decreased volume fraction solve the issues such as pressure drop. Furthermore, bigger surface area enhances the stability of the particles, resolves their settlement considerably and lowers the maintenance and transference costs of the fluids. Theoretically, the finer the particles, the bigger the surface area for transferring the heat which subsequently enhances the heat-efficiency of suspension particles as a function of heat exchange surfaces [5–15]. Choi et al. [16] conducted a numerical investigation of forced convection in a nanofluid, water–aluminum oxide, and laminar flow in a 90° bent tube.

In contrast to Newtonian fluids, the relation between shear stress and shear rate in non-Newtonian fluids is not linear. One of the common models from the numerous models which could express this behavior is the power-law model [17]. The forced convection of non-Newtonian nanofluids in a microtube under the constant temperature boundary condition was presented by Hojati et al. [18]. The results revealed higher heat exchange coefficient of nanofluids and Nusselt number compared to the basic fluid. Nusselt number of non-Newtonian nanofluid proved to be a function of Reynolds and Prandtl numbers. Shojaeian et al. [19] studied the convective heat transfer of non-Newtonian fluid flow with variable thermo-physical properties in the circular channels. Their results showed that neglecting the property variation significantly affected the heat transfer characteristics and entropy generation. Capobianchi et al. [20] investigated the heat transfer in laminar flows of extended modified power law fluids in the rectangular ducts. Etemad et al. [21] experimentally studied the viscous non-Newtonian forced convection heat transfer in the semi-circular and equilateral triangular ducts.

* Corresponding author.
E-mail address: arashkarimipour@gmail.com (A. Karimipour).

http://dx.doi.org/10.1016/j.euromechflu.2016.09.014
0997-7546/

Nomenclature

c_p	Specific heat (J kg^{-1} K^{-1})
d_p	Diameter of nanoparticles (=25 nm)
D	The diameter of microtube (m)
Kn	Knudsen number
k	Thermal conductivity (W m^{-1} K^{-1})
l	The length of microtube (m)
L	Dimensionless length of microtube in Eq. (5) ($L = l/D$)
Nu	Nusselt number
p	Pressure (Pa)
P	Pressure in non-dimensional form
Pr	Prandtl number
Re	Reynolds number
r	Radial direction (m)
R	Radial direction in non-dimensional form
T	Temperature (K)
u	Axial velocity (m s^{-1})
u_i	Inlet velocity (m s^{-1})
U	Axial velocity in non-dimensional form
u_s	Slip velocity (m s^{-1})
U_s	Slip velocity in non-dimensional form
v	Radial velocity (m s^{-1})
V	Radial velocity in non-dimensional form
x	Axial direction (m)
X	Axial direction in non-dimensional form

Greek symbols

α	Thermal diffusivity (m^2 s^{-1})
β	Slip coefficient (m)
β^*	Slip coefficient in non-dimensional form ($=\beta/D$)
γ	Shear rate (s^{-1}), $\gamma = \frac{c_p}{c_v}$ for Eq. (16)
φ	Volume fraction of nanoparticles
η	Dynamic viscosity (Ns m^{-2})
θ	Temperature in non-dimensional form
θ_s	Temperature jump in non-dimensional form
ρ	Density (kg m^{-3})

Subscripts

eff	Effective
f	Fluid
m	Averaged
nf	Nanofluid
i	Inlet condition
s	Solid nanoparticles
w	Wall

Numerous studies have been carried out to study the behavior of flow and heat transfer in the channels and microchannels. Most of these studies have been focused on the impact of Reynolds number, layout of channels cross-sections and geometric properties [22–30]. Akbarinia et al. [31] studied the forced convection of the nanofluid water–aluminum oxide in a rectangular microchannel under the slip and no-slip flow regimes. They claimed that viscosity was increased by higher volume fraction. Barkhordari et al. [32] studied the forced convection of non-Newtonian nanofluid in a microchannel under the fixed temperature and heat flux boundary conditions. They demonstrated that while Nusselt number rose, higher slip of particles slowed the convection in the tube. They also showed the effects of slip coefficient under the fixed heat flux was more significant than the fixed temperature boundary condition. Ding et al. [33] investigated the effects of Reynolds number and volume fraction on carbon nanotube forced convection under the no-slip boundary condition. They demonstrated that higher geometric ratio of the microtubes improved the heat exchange rate.

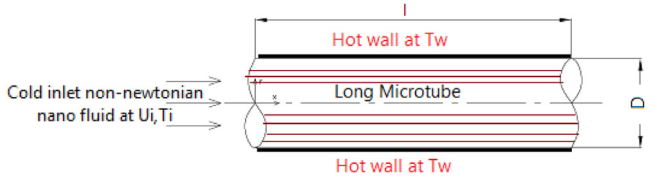

Fig. 1. Physical domain of the microtube.

Table 1
Thermo-physical properties of CMC-Al_2O_3 nanofluid.

	$\varphi = 0.005$	$\varphi = 0.015$
c_p (J/kg K)	4121	4012
k (W/mK)	0.6262	0.66
ρ (kg/m^3)	1013.5	1045.5
n (dimensionless)	0.48	0.51
K (Pa s^n)	0.22	0.24

Numerical investigation of laminar flow in a microchannel under the slip and no-slip boundary conditions of nanofluid was presented by Raisi et al. [34]; they looked at the effects of Reynolds number, volume fraction and slip velocity on heat transfer rate of forced convection flow. More works can be referred in this way [35–40].

Present study attempts to study the forced convection of non-Newtonian nanofluid laminar flow, Carboxymethyl cellulose–Aluminum oxide, in the slip flow regime through a microtube for the first time (To the author's best knowledge). The results are presented as the velocity and temperature profiles beside the averaged and local Nusselt number values.

2. Mathematical formulation

2.1. Problem statement

Fig. 1 shows the geometry of a microtube. The length and diameter of the tube are $L = 5$ mm and $D = 0.2$ mm, respectively. The length is long compared to the diameter. The cold Non-Newtonian nanofluid, Carboxyl methyl cellulose–aluminum oxide, streams along the microtube at a fixed velocity of U_i imposed to its hot wall at $T_W = 308$ K.

The diameter of the nanoparticles is 25 nm. Nanoparticles of aluminum are uniform and spherical. The flow in the microtube is laminar, non-Newtonian (pseudo-thinning plastic), incompressible and slip velocity and temperature jump boundary conditions are also considered along the microtube wall which are under the constant temperature. The radiation effects are negligible. The percentage weight of the aqueous solution of carboxy methyl cellulose–aluminum oxide is 0.5%.

The thermo-physical properties of the non-Newtonian is a pseudo-thinning plastic nanofluid at 298 K are shown in Table 1. Values of n and K (flow consistency index and index of power law) are given at 298 K for the using non-Newtonian nanofluid [41].

This research studies the fluid properties and exchange rate with Reynolds numbers at Re $= 1$, Re $= 10$ and Re $= 20$, volume fractions equal to 1.5% and 0.5%. In addition, slip velocity and temperature jump boundary conditions are considered along the microtube wall for different values of slip coefficient as $\beta^* = 0.0$, $\beta^* = 0.01$ and $\beta^* = 0.1$. As seen, index of power law of n, for the basic fluid is less than 1 which indicates that the non-Newtonian is a pseudo-thinning plastic. At present article and for the range of $0.001 < \beta^* < 0.1$ the fluid flow is considered in slip flow regime which illustrates a microflow.

2.2. Governing equations

Non-dimensional equations include continuity, momentum and energy which are formulated for steady, laminar and non-Newtonian nanofluid are as follows:

Non-dimensional continuity equation:

$$\frac{\partial U}{\partial X}+\frac{\partial V}{\partial R}=0. \tag{1}$$

Non-dimensional momentum equation along the X-direction:

$$U\frac{\partial U}{\partial X}+V\frac{\partial U}{\partial R}=-\frac{\partial P}{\partial X}+\frac{1}{\mathrm{Re}_{nf}}\times\left(\frac{\partial}{\partial X}\left(\frac{\partial U}{\partial X}\right)^{n}+\frac{\partial}{\partial R}\left(\frac{\partial U}{\partial R}\right)\right)^{n}. \tag{2}$$

Non-dimensional momentum equation along the R-direction:

$$U\frac{\partial V}{\partial X}+V\frac{\partial V}{\partial R}=-\frac{\partial P}{\partial R}+\frac{1}{\mathrm{Re}_{nf}}\times\left(\frac{\partial}{\partial X}\left(\frac{\partial V}{\partial X}\right)^{n}+\frac{1}{R}\frac{\partial}{\partial R}R\left(\frac{\partial V}{\partial R}\right)\right)^{n}-\frac{V^2}{R}. \tag{3}$$

Non-dimensional energy equation:

$$U\frac{\partial \theta}{\partial X}+V\frac{\partial \theta}{\partial R}=\frac{1}{\mathrm{Re}_{nf}\,\mathrm{Pr}_{nf}}\times\left(\frac{\partial}{\partial X}\left(\frac{\partial \theta}{\partial X}\right)^{n}+\frac{1}{R}\frac{\partial}{\partial R}R\left(\frac{\partial \theta}{\partial R}\right)\right)^{n}. \tag{4}$$

The following non-dimensional parameters have been used in Eqs. (1)–(4):

$$P=\frac{p}{\rho_{nf}u_i^2}\qquad V=\frac{v}{u_i}\qquad X=\frac{x}{D}\qquad L=\frac{l}{D}.$$
$$\theta=\frac{T-T_i}{T_w-T_i}\qquad U=\frac{u}{u_i}\qquad R=\frac{r}{D} \tag{5}$$

Reynolds number and Prandtl number are calculated by the following formulas [42].

$$\mathrm{Re}_{nf}=\frac{\rho_{nf}u_i^{2-n}D^n}{K}\qquad \mathrm{Pr}_{nf}=\frac{C_p\left(\frac{u_i}{D}\right)^{n-1}K}{k_{nf}}. \tag{6}$$

Density and heat capacity of the nanofluid can be estimated by Eqs. (7) and (8) using nanoparticles volume fraction; while the subscripts f, s and nf represent the base fluid, solid nanoparticles and nanofluid, respectively [31,43]:

$$\rho_{nf}=\varphi\rho_s+(1-\varphi)\rho_f \tag{7}$$

$$\left(\rho c_p\right)_{nf}=(1-\varphi)\left(\rho c_p\right)_f+\varphi\left(\rho c_p\right)_s. \tag{8}$$

Nanofluid thermal conductivity can be achieved from Chon et al. formula [44] (applicable for particles of 11–150 nm) which is able to consider the nanoparticles diameter and their Brownian motions as follows:

$$\frac{k_{\mathrm{eff}}}{k_f}=1+64.7\varphi^{0.7476}\left(\frac{d_f}{d_s}\right)\left(\frac{k_s}{k_f}\right)^{0.7476}\times\mathrm{Pr}^{0.9955}\,\mathrm{Re}^{1.2321}. \tag{9}$$

The power law model is used to calculate the viscosity of the nanofluid [45]:

$$\eta_{nf}=K\left(\gamma^{\cdot}\right)^{n-1} \tag{10}$$

where here $\gamma^{\cdot}$ is the shear rate.

Nanofluid thermal diffusion coefficient is demonstrated as below [46]:

$$\alpha_{nf}=\frac{k_{\mathrm{eff}}}{\left(\rho c_p\right)_{nf}}. \tag{11}$$

In the recent equation k_{eff} is the thermal conductivity coefficient.

Local Nusselt is presented as [47]:

$$\mathrm{Nu}_x=\frac{q_w''D}{k_{\mathrm{eff}}\left(T_w-T_b\right)} \tag{12}$$

where q_w'' is the wall heat flux, T_b is the bulk temperature and T_w is the wall temperature.

For the averaged Nusselt, the following equation is used [47]:

$$\mathrm{Nu}_m=\frac{1}{L}\int_0^L \mathrm{Nu}_x\,dx. \tag{13}$$

2.3. Boundary conditions

No slip boundary condition and lack of temperature jump may not be suitable for microscales flows. At slip flow regimes, there is a region in which fluid molecules oscillate. This region whose thickness is in proportion to molecular mean free path is called Knudsen layer. The effects of Knudsen layer are negligible but must be considered in slip regimes as the slip boundary condition between fluid and the solid boundary may reflect the impact of activities and levels of molecular particles. Slip velocity and temperature jump are quantified via relations [48,49].

Slip velocity values can be determined along the walls by:

$$u_s=-\frac{2-F_m}{F_m}\beta\left(\frac{\partial u}{\partial r}\right)_{r=r_0}. \tag{14}$$

β, u_s and F_m are slip velocity coefficient, slip velocity and adaptation coefficient, respectively. Adaptation coefficient is chosen as 1. The non-dimensional slip velocity is achieved as:

$$U_s=-\beta^*\left(\frac{\partial U}{\partial R}\right)_{R=R_0}. \tag{15}$$

R_0 is the dimensionless microtube radius and β^* represents the non-dimensional slip velocity coefficient which is defined as $\beta^*=\frac{\beta}{D}$. Moreover, the temperature jump values can be determined along the microtube wall [50,51]:

$$T_s-T_w=-\frac{2-F_t}{F_t}\frac{2\gamma}{\gamma+1}\frac{\beta}{\mathrm{Pr}}\left(\frac{\partial T}{\partial r}\right)_{r=r_0} \tag{16}$$

where for the temperature boundary condition, $\gamma=\frac{c_p}{c_v}$, T_s, T_w and F_t are special heat, temperature jump, wall temperature and thermal adaptation coefficient (=1), respectively.

The non-dimensional form of temperature jump is presented by Eq. (17)

$$\theta_s-\theta_w=-\frac{\beta^*}{\mathrm{Pr}}\left(\frac{\partial \theta}{\partial R}\right)_{R=R_0}. \tag{17}$$

3. Numerical procedure, grid independency and validation

The numerical finite volume method (FVM) on the non-uniform staggered mesh according to the SIMPLE algorithm is used to couple the velocity–pressure correction equations. Moreover the second order upwind scheme is applied to discretize the diffusion and convective terms. The time division multiple access method

Table 2
Grid independency study for the values of U and θ at $X = L/2$ and $R = 0$ at $\varphi = 0.005$, Re $= 1$ and $\beta = 0.0$ for CMC-Al_2O_3 nanofluid.

	750 × 30	1000 × 40	1250 × 50
U	1.6458	1.6464	1.6468
θ	0.8905	0.8906	0.8906

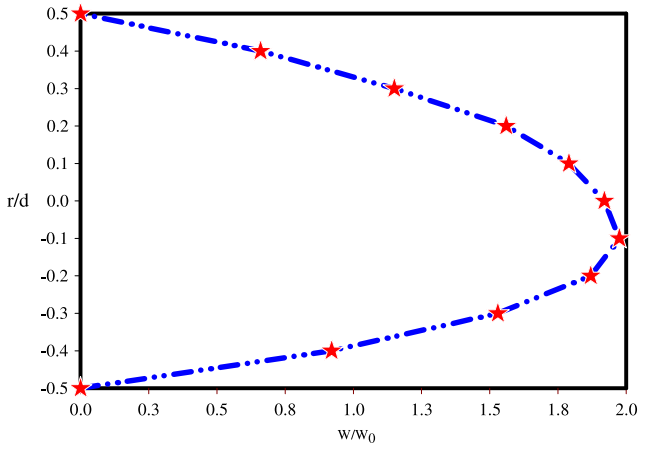

Fig. 2. Dimensionless fully developed axial velocity profiles from the present work versus Akbari et al. [52] (Symbols: Akbari et al., Lines: Present work).

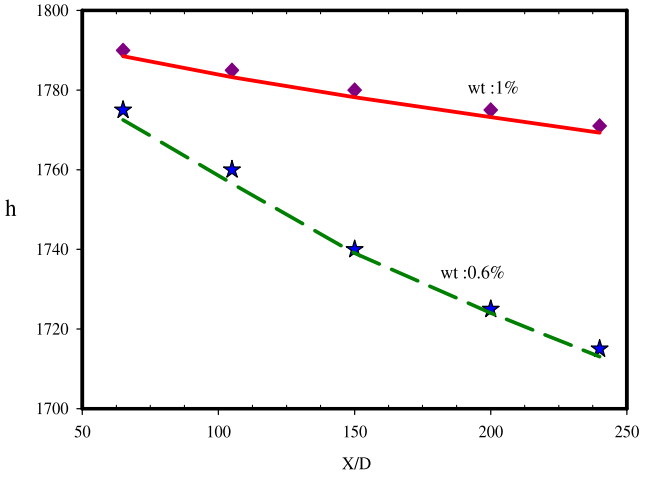

Fig. 3. Effects of particles volume fraction on heat transfer coefficient at Re $= 1550$ with Keshavarz et al. [17] (Symbols: Keshavarz et al., Lines: Present work).

(TDMA) is used to solve the implicit system of equations for any of the unknown variables.

The values of U and θ at $X = L/2$ and $R = 0$ for $\varphi = 0.005$, Re $= 1$, and $\beta^* = 0.0$ and for CMC-Al_2O_3 nanofluid at different grid nodes are presented in Table 2. Difference between the results of 1000 × 40 and 1250 × 50 are found negligible; so the grid of 1000 × 40 is chosen for the next calculations.

For validation, developed velocity profiles of water–aluminum oxide inside a tube with Gr $= 5 \times 10^5$ and $\varphi = 2\%$ values are compared with those of Akbari et al. [52] in Fig. 2.

More validation which concerns the heat transfer rate of xanthan–aluminum oxide (a non-Newtonian nanofluid) inside a tube with a volume fraction of 4% and Re $= 1510$ are compared with those of Keshavarz et al. [17] in Fig. 3.

At last, the fully developed velocity profiles of water–aluminum oxide inside a microchannel with Re $= 50$ and $\varphi = 3\%$ in the slip flow regime, are presented versus Raisi et al. [34] in Fig. 4. Suitable agreements are observed in all of these figures.

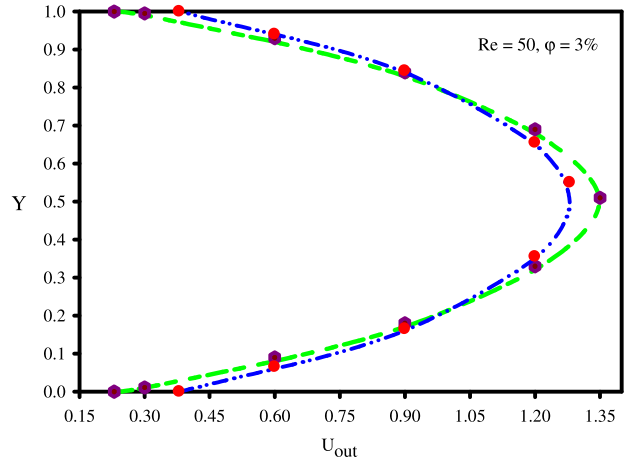

Fig. 4. Effects of slip velocity coefficient on the outlet velocity profile at Re $= 50$ and $\varphi = 3\%$ with Raisi et al. [34] (Symbols: Raisi et al., Lines: Present work).

4. Results and discussion

This study investigates the forced convection of heat of a nanofluid inside a horizontal microtube with Re $= 1$, Re $= 10$ and Re $= 20$ and volume fractions equal to 1.5% and 0.5%. In addition, slip velocity and temperature jump boundary conditions are considered along the microtube wall for different values of slip coefficient as $\beta^* = 0.0$, $\beta^* = 0.01$ and $\beta^* = 0.1$. To solve the governing Navier–Stokes equations and discretization of the solution domain, the numerical method of finite volume and SIMPLE algorithm are employed according to the second order upwind scheme.

As Fig. 1 shows, the hot wall of the tube is exposed to $T_W = 308$ K. The cold Non-Newtonian nanofluid Carboxyl methyl cellulose–aluminum oxide is injected into the microtube at the temperature 298 K and fixed velocity of u_i and exits at the other end of the tube. Slip velocity and temperature jump boundary conditions are considered along the walls.

Fig. 5 shows the fully developed horizontal velocity profiles of U for CMC-Al_2O_3 nanofluid at $\varphi = 0.015$, Re $= 10$ for different values of β^*. Slip coefficient β^* has the significant effects on U profiles from $\beta^* = 0.0$ to $\beta^* = 0.1$. It is seen that more β^* corresponds to more velocity at $R = 0$ and $R = 1$ and less U_{max} at $R = 0.0$. In this diagram, nanofluid flow is developed in form of parabolic profiles and gains velocity on the wall because of occurrence of slip boundary condition. For the non-Newtonian laminar flow, higher slip coefficient results into increased non-Newtonian nanofluid velocity along the wall. With regard to Fig. 5 and for each slip coefficients, start point of the diagram is difference between the parabolic velocity profiles which is indicated with an arrow in this figure. For these low values of concentration and Reynolds number ($\varphi = 0.015$ and Re $= 10$), it is worth noting that the velocity profile represents the typical of non-Newtonian laminar flow for the state of $\beta^* = 0$ (nonslip boundary condition) so that the effect of nanofluid as a non-Newtonian agent can be clearly observed; However the velocity profile again becomes parabolic at higher slip coefficient due to existence the slip velocity on the wall which is the typical of Newtonian laminar flow.

Temperature profiles of θ along the vertical centerline of microtube ($X = L/2$) at $\varphi = 0.015$, Re $= 10$ for different values of β^* are shown in Fig. 6. Due to occurrence of the temperature jump on the wall, nanofluid temperature on the wall of the tube is not equal with the wall temperature. The effects of temperature jump can be ignored due to being far away from the microtube entrance. Nanofluid temperature tends to the wall's one along the tube which means low values of temperature jump are achieved with X. Moreover higher amounts of slip coefficient leads to

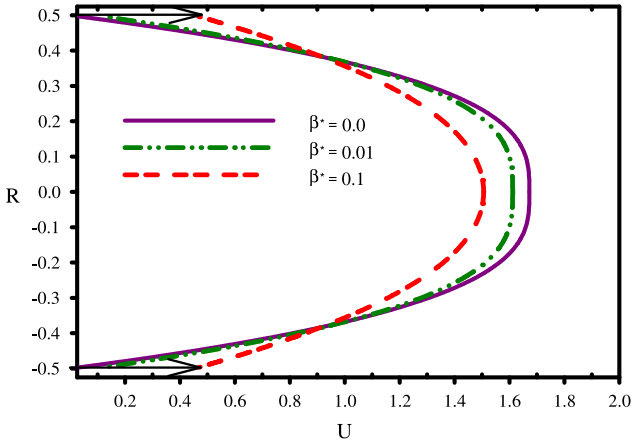

Fig. 5. Fully developed horizontal velocity profiles along the microtube vertical centerline for CMC-Al_2O_3 nanofluid at $\varphi = 0.015$ and Re $= 10$ for different values of β^*.

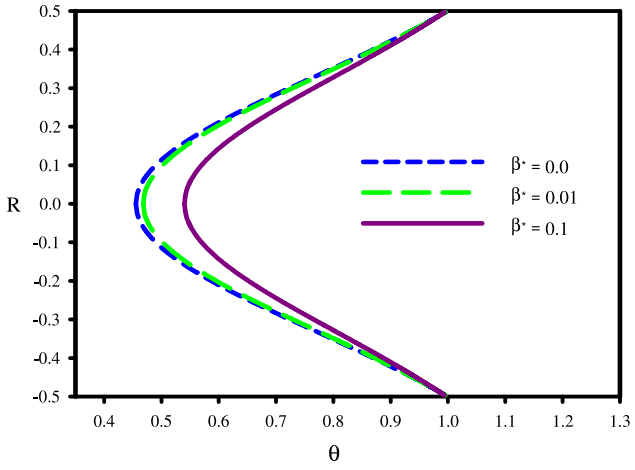

Fig. 6. Temperature profiles of θ at microtube vertical centerline for CMC-Al_2O_3 nanofluid at $\varphi = 0.015$ and Re $= 10$ for different values of β^*.

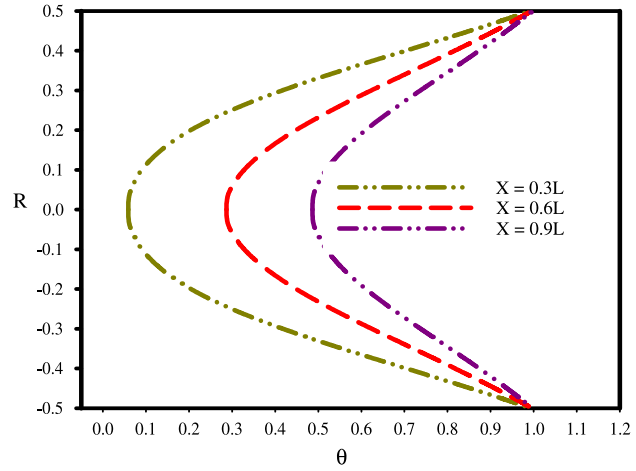

Fig. 7. Temperature profiles of θ at different cross sections of microtube for CMC-Al_2O_3 nanofluid at $\varphi = 0.015$ and Re $= 10$ for $\beta^* = 0.1$.

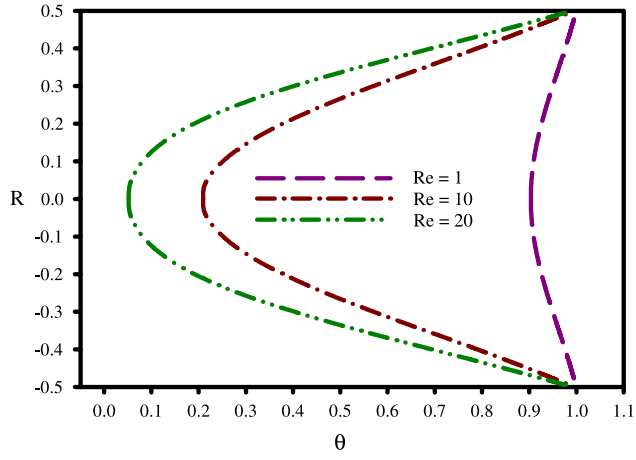

Fig. 8. Temperature profiles of θ at microtube vertical centerline for CMC-Al_2O_3 nanofluid at $\varphi = 0.015$ and $\beta^* = 0.1$ for different values of Re.

more temperature of nanofluid imposed to the hot wall. This phenomenon implies larger heat transfer rate from the solid wall to the inside fluid due to existence the slip velocity along the wall.

Temperature profiles of θ at different cross sections of microchannel for CMC-Al_2O_3 nanofluid at $\varphi = 0.015$, Re $= 10$, for $\beta^* = 0.1$ are observed in Fig. 7. This figure indicates that, as expected, higher X leads to higher non-dimensional temperature in the centerline of the microtube. The inlet nanofluid is heated by the heat exchange with the hot microtube wall through the microtube so that at $X = 0.9L$ the nanofluid temperature would be almost equal to the wall temperature.

Fig. 8 shows the impacts of the Reynolds number on temperature profile (θ) at ($X = L/2$), $\varphi = 0.015$ and $\beta^* = 0.1$. There is less time at higher Re for heat exchange between the wall and the nanofluid. As Reynolds number increases, the velocity profiles undergo change significantly. Moreover existence the temperature jump along the wall means the nanofluid temperature on the wall is not equal with the wall temperature and leads to achieve more temperature at the middle of the tube for higher values of slip coefficient which means the length of the thermal developing region (entrance length) increases with volume fraction, Reynolds number and slip coefficient, respectively. It is well known that the length of the thermal developing region increases with Reynolds number. By using nanoparticles suspended in the basic fluid and higher volume fraction of them, the non-dimensional temperature of the nanofluid raises due to increased heat conduction coefficient; However the thermal entrance length can be determined by $L_t = C_t D$ Re Pr which C_t is the thermal entrance length coefficient [53,54]. It is seen that higher volume fraction results into more Prandtl number; then higher Prandtl number leads to longer thermal entrance length. This fact can be seen at present paper as follows:

For the state of Re $= 10$, $\varphi = 0.5\% \Rightarrow$ Pr $= 33.33 \Rightarrow L_t =$ 2.2 mm.

For the state of Re $= 10$, $\varphi = 1.5\% \Rightarrow$ Pr $= 39.38 \Rightarrow L_t =$ 2.6 mm.

Moreover existence the temperature jump means the nanofluid temperature on the wall is not equal with the wall one and leads to achieve more temperature at the middle of the tube for higher values of slip coefficient. This means the length of the thermal developing region (entrance length) increases with all volume fraction, Reynolds number and slip coefficient.

One of the most noticeable properties of the supposed flow is existence the slip velocity which leads the fluid on the wall slip along it with different velocity. This phenomenon can be observed in Fig. 9 which concerns the slip velocity profiles along the microtube wall for different values of β^* at $\varphi = 0.015$ and Re $=$ 10. The profile begins from its greatest amount at inlet and then it reduces along the microtube wall so that tends to the specified value. This figure implies the significant effects of β^* on U_s. The diagram holds that the slip velocity of the wall is at maximum

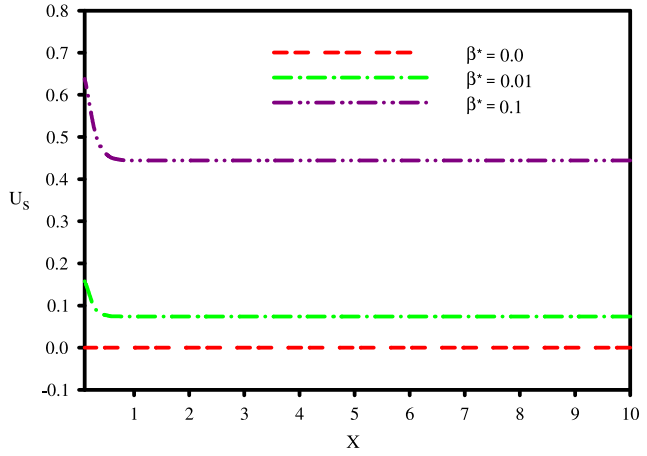

Fig. 9. Slip velocity profiles for CMC-Al_2O_3 nanofluid along the microtube wall at $\varphi = 0.015$ and Re $= 10$ for different values of β^*.

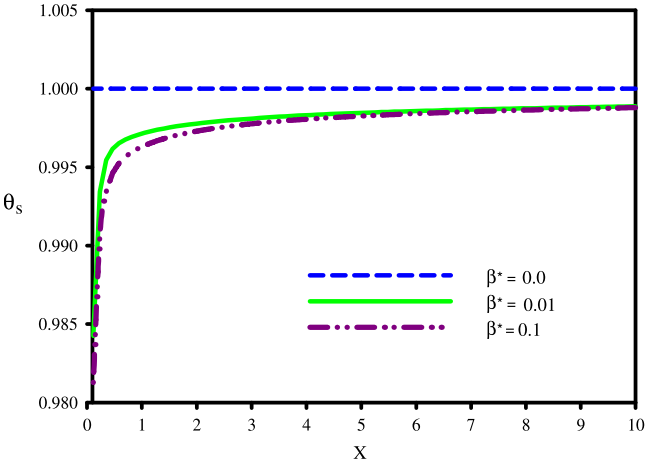

Fig. 10. Temperature jump for CMC-Al_2O_3 nanofluid along the microtube wall at $\varphi = 0.015$ and Re $= 10$ for different values of β^*.

at the entrance point of the tube. Slip coefficient significantly affects the slip velocity of the nanofluid, so that as slip coefficient increases, the flow tends to the slip regime and enhances the slip velocity along the wall (slip velocity is zero at $\beta^* = 0.0$).

Temperature jump variations along the microtube wall are presented in Fig. 10 for CMC-Al_2O_3 nanofluid at $\varphi = 0.015$, Re $=$ 10 and different values of β^*. The effects of temperature jump are ignored in the most previous articles; however this figure implies that its values are sensible at entrance region where involves the most heat exchange with the wall. The diagram shows that higher slip coefficient raises the temperature jump. However, the rate is diminished along the tube. Nanofluid temperature is the same of the temperature of the wall at $\beta^* = 0.0$.

Nusselt numbers of the nanofluid on the walls for different slip coefficients are presented in Fig. 11. This figure displays the effect of different β^* on Nu_X along the wall at Re $=$ 1, 10, 20 and $\phi =$ 1.5%. The tube Nusselt number has been calculated as Nu $= 3.657$ under the constant temperature boundary condition in a fully developed laminar flow; but due to existence the nanoparticles, slip coefficient and non-Newtonian nature of the fluid, Nusselt number would not equal to 3.657 any longer.

Moreover local Nusselt number for CMC-Al_2O_3 nanofluid along the microtube wall at different values of Re for $\varphi = 0.015$, $\beta^* =$ 0.1 are shown in Fig. 12. The results indicate that higher Reynolds number results in higher Nusselt number as it is well known.

To better explain the heat transfer rate from the wall, the averaged Nusselt number of the nanofluid is given in Fig. 13 for

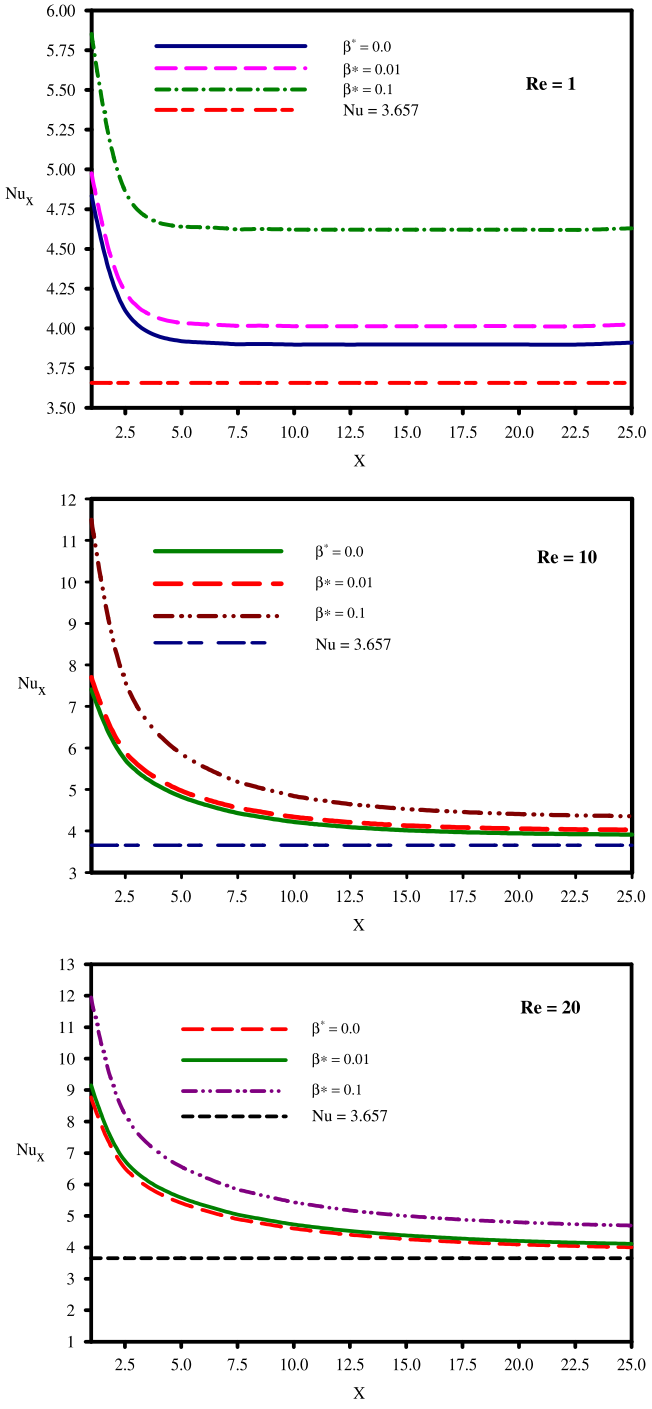

Fig. 11. Nu_X along the microtube wall at different values of β^* and Re for $\varphi =$ 0.015.

different slip coefficients and different volume fractions. Higher slip coefficient leads to higher Nusselt number especially at more Re which means averaged Nusselt number increases due to slip flow regime. The results also indicate that larger Reynolds number leads to larger averaged Nusselt number.

5. Conclusions

This study attempted to study the forced convection of the non-Newtonian nanofluid CMC–aluminum oxide under the slip flow regime. The effects of nanoparticle concentrations, slip coefficient were investigated on the flow field and heat transfer. Maximum

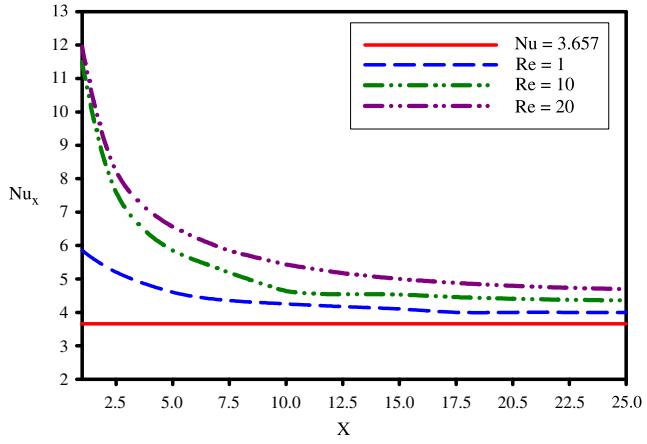

Fig. 12. Nu_X along the microtube wall at different values of Re for $\varphi = 0.015$ and $\beta^* = 0.1$.

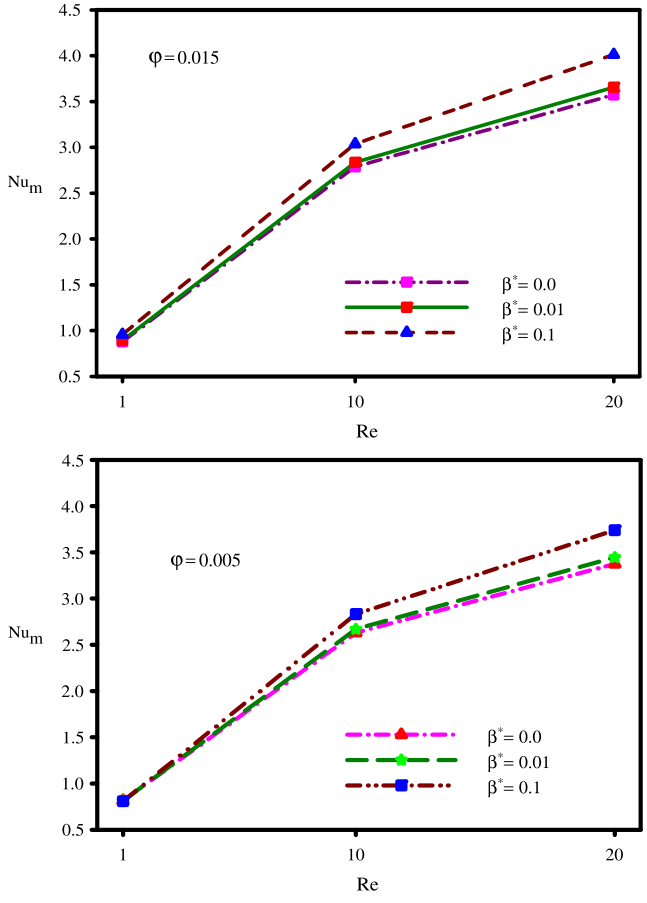

Fig. 13. Nu_m on the microtube wall for different values of Re and β^* at $\varphi = 0.015$ and $\varphi = 0.005$.

Nusselt number occurred at the entrance region of the microtube and approached to the fixed value along the tube asymptotically in a descending trend. Slip coefficient significantly affected the slip velocity and temperature jump of the nanofluid. More slip coefficient β^* corresponded to larger Nu_m. The Temperature jump effects should be involved at microtube entrance area where the most heat exchange with the wall happened. Larger β^* corresponded to larger θ_s. The tube Nusselt number has been calculated as $Nu = 3.657$ under the constant temperature boundary condition in a fully developed laminar flow; but due to existence the nanoparticles, slip coefficient and non-Newtonian nature of the fluid, Nusselt number would not equal to 3.657 any longer. Moreover higher slip coefficient led to higher Nusselt number especially at more Re which meant averaged Nusselt number increased due to slip flow regime.

References

[1] A. Karimipour, A. Hossein Nezhad, A. D'Orazio, M. Hemmat Esfe, M. Safaei, E. Shirani, Simulation of copper–water nanofluid in a microchannel in slip flow regime using the lattice Boltzmann method, Eur. J. Mech. B/Fluids 49 (2015) 89–99.

[2] A. Karimipour, A. Hossein Nezhad, A. D'Orazio, E. Shirani, Investigation of the gravity effects on the mixed convection heat transfer in a microchannel using lattice Boltzmann method, Int. J. Therm. Sci. 54 (2012) 142–152.

[3] A. Karimipour, A.H. Nezhad, A. D'Orazio, E. Shirani, The effects of inclination angle and Prandtl number on the mixed convection in the inclined lid driven cavity using lattice Boltzmann method, J. Theoret. Appl. Mech. 51 (2013) 447–462.

[4] A. Karimipour, M.H. Esfe, M.R. Safaei, D. Toghraie, S.N. Kazi, Mixed convection of Copper-Water nanofluid in a shallow inclined lid driven cavity using lattice Boltzmann method, Physica A 402 (2014) 150–168.

[5] M.R. Safaei, O. Mahian, F. Garoosi, K. Hooman, A. Karimipour, S.N. Kazi, S. Gharehkhani, Investigation of micro and nano-sized particle erosion in a 90° pipe bend using a two-phase discrete phase model, Sci. World J. 2014 (2014) 11. Article ID 740578.

[6] Mohammad Reza Safaei, Goodarz Ahmadi, Mohammad Shahab Goodarzi, Mostafa Safdari Shadloo, Hamid Reza Goshayeshi, Mahidzal Dahari, Heat transfer and pressure drop in fully developed turbulent flows of graphene nanoplatelets–silver/water nanofluids, Fluids (1) (2016) 20. http://dx.doi.org/10.3390/fluids1030020.

[7] Raffaele Ardito, Alberto Corigliano, Attilio Frangi, Modelling of spontaneous adhesion phenomena in micro-electro-mechanical systems, Eur. J. Mech.-A/Solids 39 (2013) 144–152.

[8] M.H. Esfe, A.A.A. Arani, A. Karimipour, S.S.M. Esforjani, Numerical simulation of natural convection around an obstacle placed in an enclosure filled with different types of nanofluids, Heat Transfer Res. 45 (3) (2014) 279–292.

[9] M.A. Sheremet, S. Dinarvand, I. Pop, Effect of thermal stratification on free convection in a square porous cavity filled with a nanofluid using Tiwari and Das' nanofluid model, Physica E 69 (2015) 332–341.

[10] A. Akbarinia, R. Laur, Investigating the diameter of solid particles effects on a laminar nanofluid flow in a curved tube using a two phase approach, Int. J. Heat Fluid Flow 30 (2009) 706–718.

[11] A. Malvandi, D.D. Ganji, Effects of nanoparticle migration and asymmetric heating on magnetohydrodynamic forced convection of alumina/water nanofluid in microchannels, Eur. J. Mech. B/Fluids 52 (2015) 169–184.

[12] M. Hemmat Esfe, M. Akbari, A. Karimipour, M. Afrand, O. Mahian, S. Wongwises, Mixed convection flow and heat transfer in an inclined cavity equipped to a hot obstacle using nanofluids considering temperature-dependent properties, Int. J. Heat Mass Transfer 85 (2015) 656–666.

[13] A. Santra, S. Sen, N. Chakraborty, Study of heat transfer due to laminar flow of copper–water nanofluid through two isothermally heated parallel plates, Int. J. Therm. Sci. 48 (2009) 391–400.

[14] A. Behzadmehr, M. Saffar-Avval, N. Galanis, Prediction of turbulent forced convection of a nanofluid in a tube with uniform heat flux using a two phase approach, Int. J. Heat Fluid Flow 28 (2007) 211–219.

[15] M.H. Esfe, M. Akbari, D. Toghraie, A. Karimipour, M. Afrand, Effect of nanofluid variable properties on mixed convection flow and heat transfer in an inclined two-sided lid-driven cavity with sinusoidal heating on sidewalls, Heat Transfer Res. 45 (2014) 409–432.

[16] J. Choi, Y. Zhang, Numerical simulation of laminar forced convection heat transfer of Al2O3–water nanofluid in a pipe with return bend, Int. J. Therm. Sci. 55 (2012) 90–102.

[17] M. Keshavarz, S.M. Hossein Haddad, M. Darabi, Modeling of force convection heat transfer of a non-Newtonian nanofluid in the horizontal tube under constant heat flux with computational fluid dynamics, Int. Commun. Heat Mass Transfer 39 (2012) 995–999.

[18] M. Hojati, S.G.H. Etemad, R. Bagheri, J. Thibault, Convection heat transfer of non-Newtonian nanofluid through a uniformly circular tube, Exp. Therm Fluid Sci. 35 (2011) 1351–1356.

[19] M. Shojaeian, M. Yildiz, A. Kosar, Convective heat transfer and second law analysis of non-Newtonian fluid flows with variable thermophysical properties in circular channels, Int. Commun. Heat Mass Transfer 60 (2015) 21–31.

[20] M. Capobianchi, D. Wagner, Investigated the heat transfer in laminar flows of extended modified power law fluids in rectangular ducts, Int. J. Heat Mass Transfer 53 (2010) 558–563.

[21] S.G.H. Etemad, A.S. Mujumdar, R. Nassef, Viscous non-Newtonian forced convection heat transfer I semi-circular and equilateral triangular ducts, Int. Commun. Heat Mass Transfer 24 (1997) 609–620.

[22] Mohammad Reza Safaei, Marjan Gooarzi, Omid Ali Akbari, Mostafa Safdari Shadloo, Mahidzal Dahari, Performance evaluation of nanofluids in an inclined ribbed microchannel for electronic cooling applications, in: Book Chapter in Electronic Cooling, INTECH Publication, 2016, http://dx.doi.org/10.5772/62898.

[23] K. Pawan Singh, P.V. Harikrishna, T. Sundararajan, K. Sarit Das, Experimental and numerical investigation into the hydrodynamics of nanofluids in microchannels, Exp. Therm Fluid Sci. 42 (2012) 174–186.
[24] J. Jung, H. Oh, H. Kwak, Forced convective heat transfer of nanofluids in microchannels, Int. J. Heat Mass Transfer 52 (2009) 466–472.
[25] S.M. Aminossadati, A. Raisi, B. Ghasemi, Effect of magnetic field on nanofluid forced convection in a partially heated microchannel, Int. J. Non-Linear Mech. 46 (2011) 1373–1382.
[26] M. Shariat, A. Akbarinia, A. HosseinNezhad, A. Behzadmehr, R. Laur, Numerical study of two phase laminar mixed convection nanofluid in elliptic ducts, Appl. Therm. Eng. 31 (2011) 2348–2359.
[27] M. Gad-el-Hak, Flow physics in MEMS, Rev. Mech. Ind. 2 (2001) 313–341.
[28] T.M. Adams, S.I. Abdel-Khalik, S.I. Jeter, Z.H. Qureshi, An experimental investigation of single-phase forced convection in microchannel, Int. J. Heat Mass Transfer 41 (1998) 851–857.
[29] Y. Xuan, Q. Li, M. Ye, Investigation of convection heat transfer in ferrofluid microflows using lattice-Boltzmann approach, Int. J. Therm. Sci. 46 (2007) 105–111.
[30] C. Ho, Y. Tia, Micro-electro-mechanical-system (MEMS) and fluid flows, Annu. Rev. Fluid Mech. 30 (1998) 579–612.
[31] A. Akbarinia, M. Abdolzadeh, R. Laur, Critical investigation of heat transfer enhancement using nanofluids in microchannels with slip and non-slip flow regimes, Appl. Therm. Eng. 31 (2011) 556–565.
[32] M. Barkhordari, S.G.H. Etemad, Numerical study of slip flow heat transfer of non-Newtonian fluids in circular microchannels, Int. J. Heat Fluid Flow 28 (2007) 1027–1033.
[33] Y. Ding, H. Alias, D. Wen, R. Williams, Heat transfer of aqueous suspension of carbon nanotube, Int. J. Heat Mass Transfer 49 (2006) 240–250.
[34] A. Raisi, B. Ghasemi, S.M. Aminossadati, A numerical study on the forced convection of laminar nanofluid in a microchannel with both slip and no-slip conditions, Int. J. Comput. Methodol. 59 (2012) 114–129.
[35] M. Rahman, M.A. Al-Lawatia, I.A. Eltayeb, N. Al-Salti, Hydromagnetic slip flow of water based nanofluids past a wedge with convective surface in the presence of heat generation or absorption, Internat. J. Non-Linear Mech. 46 (2011) 1373–1382.
[36] A. Karimipour, A.H. Nezhad, A. Behzadmehr, S. Alikhani, E. Abedini, Periodic mixed convection of a nanofluid in a cavity with top lid sinusoidal motion, Proc. Inst. Mech. Eng, Part C: J. Mech. Eng. Sci. 225 (2011) 2149–2160.
[37] H. Afshar, M. Shams, S.M.M. Nainian, G. Ahmadi, Microchannel heat transfer and dispersion of nanoparticles in slip flow regime with constant heat flux, Int. Commun. Heat Mass Transfer 36 (2009) 1060–1066.
[38] M. Kalteh, A. Abbassi, M. Saffar-Avval, J. Harting, Eulerian-Eulerian two-phase numerical simulation of nanofluid laminar forced convection in a microchannel, Int. J. Heat Fluid Flow 32 (2011) 107–116.
[39] Mohammad Mehdi Rashidi, Mohmmad Nasiri, Mostafa Safdari Shadloo, Zhighang Yang, Entropy generation in a circular tube heat exchanger using nanofluids: Effects of different modeling approaches, Heat Transfer Eng., in press. http://dx.doi.org/10.1080/01457632.2016.1211916.
[40] A. Karimipour, New correlation for Nusselt number of nanofluid with $Ag/AL_2O_3/Cu$ nanoparticles a microchannel considering slip velocity and temperature jump by using Lattice Boltzmann method, Int. J. Thermal Sci. 91 (2015) 146–156.
[41] M. Hojati, S.G.H. Etemad, R. Bagheri, J. Thibault, Rheological characteristics of non-Newtonian nanofluids: Experimental investigation, Int. Commun. Heat Mass Transfer 38 (2011) 144–148.
[42] R. Shyam, R.P. Chhabra, Effect of Prandtl number on heat transfer from tamdem square cylinders immersed in power-law fluids in the low Reynolds number regime, Int. J. Heat Mass Transfer 57 (2013) 742–755.
[43] J.C. Han, Y.M. Zhang, High performance heat transfer ducts with parallel broken and V-shaped broken ribs, Int. J. Heat Mass Transfer 35 (1992) 513–523.
[44] C.H. Chon, K.D. Kihm, S.P. Lee, S.U.S. Choi, Empirical correlation finding the role of temperature and particle size for nanofluid (AL2O3) thermal conductivity enhancement, Appl. Phys. Lett. 87 (2005) 1–3.
[45] R. Kamali, A.R. Binesh, Numerical investigation of heat transfer enhancement using carbon nanotube non-Newtonian nanofluids, Int. Commun. Heat Mass Transfer 37 (2010) 1153–1157.
[46] H.C. Brinkman, The viscosity of concentrated suspensions and solution, J. Chem. Phys. 20 (1952) 571–581.
[47] S. Mirmasomi, A. Behzadmehr, Numerical study of laminar mixed convection of a nanofluid in a horizontal tube using two-phase mixture model, Appl. Therm. Eng. 28 (2007) 717–727.
[48] N.G. Hadjiconstantinou, O. Simek, Constant-wall-temperature Nusselt number in micro nano-channels, Trans. ASME 124 (2002) 356–364.
[49] A. Beskok, G.E. Karniadakis, Simulation of heat and momentum transfer in complex microgeometries, J. Thermophys. Heat Transfer 8 (1994) 647–655.
[50] A.K. Satapathy, Slip flow heat transfer in an infinite microube with axial conduction, Int. J. Therm. Sci. 49 (1) (2010) 153–160.
[51] V. Vandadi, A. Vandadi, C. Aghanajafi, Slip-Flow heat transfer circular microchannel with viscous dissipation, IJRRAS 6 (2011) 176–181.
[52] M. Akbari, A. Behzadmehr, F. Shahraki, Fully developed mixed convection in horizontal and inclined tubes with uniform heat flux using nanofluid, Int. J. Heat Fluid Flow 29 (2008) 545–556.
[53] L.M. Jiji, Heat Convection, second ed., Springer-Verlag, Berlin, Heidelberg, 2009.
[54] A. Bejan, Convection Heat Transfer, third ed., Wiley, 2004.